

Filtrated Grouping in Multiple Functional Regression

Shuhao Jiao^{*1}, Hernando Ombao², and Ian W. McKeague³

¹Department of Biostatistics, City University of Hong Kong

²Statistics Program, KAUST, Saudi Arabia

³Department of Biostatistics, Columbia University

Abstract

To understand and communicate the risk of chronic joint disease associated with aging, it is essential to investigate how age is associated with gait patterns, particularly through gait angular kinematics. Motivated by this need, and by the critical role of joint coordination in gait, we propose a novel covariate grouping framework within the context of multiple functional regression, where a scalar response is linked to multiple functional covariates. We apply this approach to investigate the relationship between chronological age and gait angular kinematics, aiming to uncover biomechanical patterns that signal age-related gait pattern evolution. Specifically, we develop a forest-structured covariate grouping framework in which different functional covariates are aggregated hierarchically based on the level of coefficient homogeneity. This approach allows for the analysis of both common and idiosyncratic effects of covariates in a nuanced, multi-resolution manner. The identification of the forest structure is entirely data-driven and requires no prior knowledge, providing valuable insights into the interdependence among covariates. Compared to existing methods, the proposed regression framework demonstrates superior predictive power and offers more insightful interpretability on joint coordination. In addition, the proposed framework is broadly applicable and can be readily extended to analyze multivariate functional data in other scientific domains.

Keywords: Angular kinematics, Effective age, Filtrated grouping, Multiple functional regression, Partial least squares.

^{*}Corresponding Author: shuhao.jiao@cityu.edu.hk

1 Introduction

1.1 Backgrounds and Objectives

Gait analysis (GA) is a widely utilized method for examining and understanding angular kinematics, which involves studying the rotational movements of joints during activities such as walking. This analysis provides valuable insights into joint function and coordination, aiding in the assessment of movement patterns and the identification of potential abnormalities (see e.g., Kay et al. [20], Lofterød et al. [25] and Rao et al. [32]). The study in this paper is driven by a growing scientific interest in the intersection of chronic risk communication and gait analysis.

As individuals age, changes in joint flexibility, muscle strength, and neuromuscular control can alter these angular movements, leading to decreased mobility and increased fall risk. An emerging concept, referred to as “effective age” has garnered increasing attention in recent years (see e.g., Anderson and Loeser [1], Loeser [24], Li et al. [23], and Spiegelhalter [36]). Effective age represents the age of a “healthy” individual who shares the same risk profile as a person being evaluated. In many cases, a person’s health status is more accurately reflected by their effective age rather than their chronological age, as it accounts for the impact of chronic disease risks and overall well-being. Evaluating effective age through gait analysis is a vital component in the proactive management of joint health, facilitating early detection of degeneration, customization of rehabilitation strategies, and the promotion of sustained mobility and independence.

Here we analyze a dataset generated from the experiment conducted by Fukuchi et al. [14]. The study involves 42 healthy volunteers aged between 21 and 84, all of whom had no lower-extremity injuries in the six months prior to participation and no orthopedic or neurological conditions affecting their gait. Studying the association between chronological age and gait angular kinematics in healthy individuals is essential, as it serves as a baseline for assessing new subjects. Data were collected using standard gait-analysis procedures in a 10m \times 12m room equipped with 12 cameras, five force platforms embedded in the floor, and a dual-belt instrumented treadmill. This study focuses on treadmill walking data, as they offer greater consistency and are not influenced by terrain variations. The angular kinematics were recorded at various gait speeds, categorized into eight groups (S1 — S8) ranging from the slowest to the fastest speeds. The ensemble averages of angular kinematics across different speed levels are shown in Figure 1. We develop an innovative tool to study the association between joint angular kinematics and chronological age, as a building block for effective age evaluation. *To achieve this, we employ multiple functional regression, where age serves as the response variable and angular kinematics curves are the predictors.*

1.2 Functional Linear Regression and Covariate Grouping

Multivariate functional data analysis (FDA) offers a powerful toolbox for handling multiple complex functional objects. Its primary strength lies in addressing the dual challenges of high dimensionality inherent in individual functional objects and the intricate interdependence among them. Recent advancements in this field have enabled

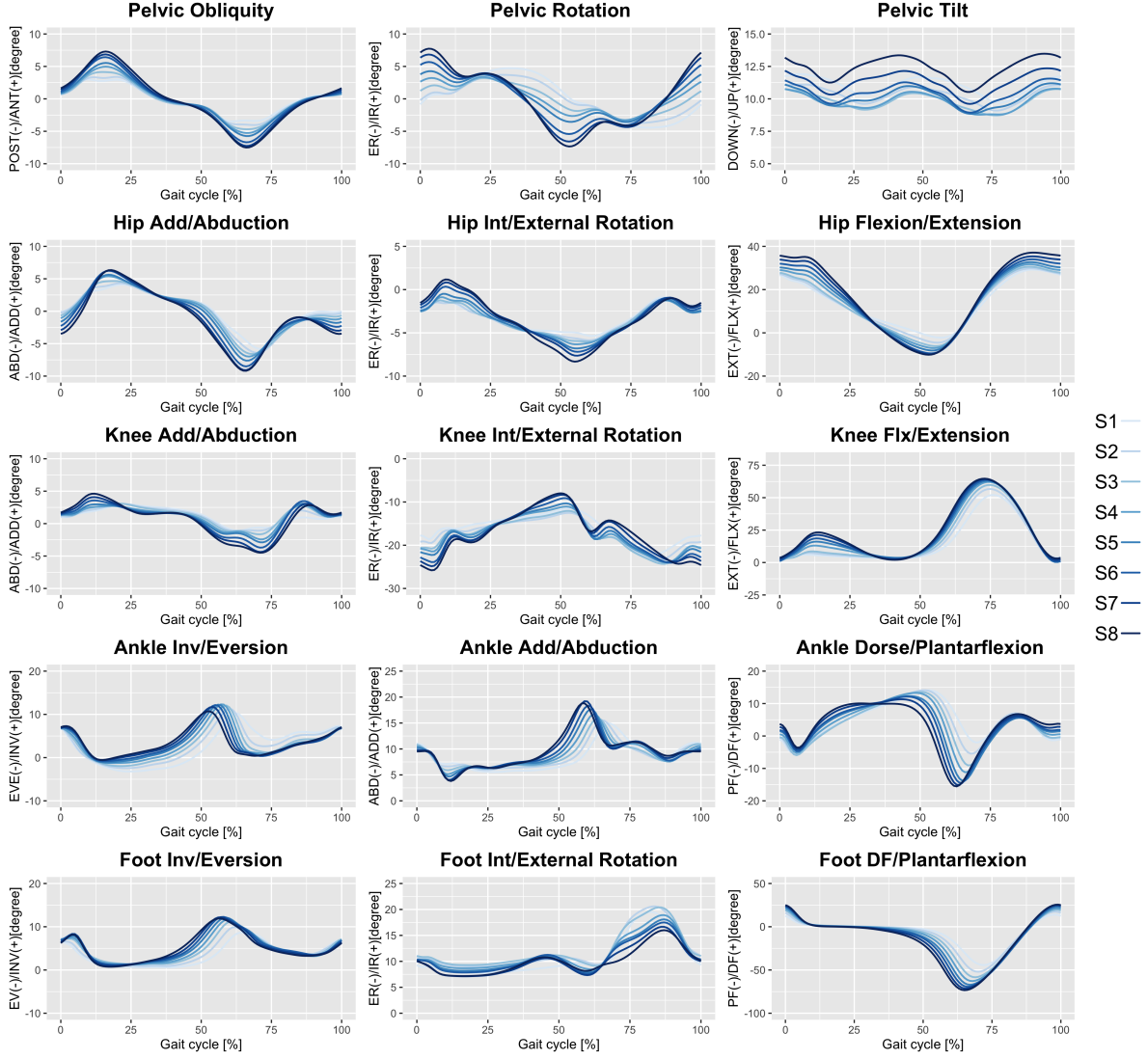


Figure 1: Angular kinematics during treadmill walking averaged over different levels of gait speed (right-hand side). S5 represents the comfortable walking speed.

researchers to tackle diverse challenges across various domains, including neuroimaging analysis (e.g., Wang et al. [37] and Jiao et al. [18]), public health (e.g., Zhou et al. [41]), and gait analysis (e.g., Cheng et al. [3], Dannenmaier et al. [7], and Cao et al. [2]). These developments underscore the versatility and potential of multivariate FDA in addressing complex, high-dimensional problems across diverse domains. Among its various tools, functional linear regression (see Ramsay and Silverman [31] and Morris [27] for overviews) stands out as a well-established class of linear models. In this article, we focus on the following model with a scalar response $y_n \in \mathbb{R}$ and multiple functional covariates $\{X_{jn}(t) \in L^2[0, 1]: j = 1, \dots, p\}$,

$$y_n = \beta_0 + \sum_{j=1}^p \langle X_{jn}, \beta_j \rangle + \epsilon_n, \quad E\epsilon_n = 0, \quad \text{Var}(\epsilon_n) = \sigma^2, \quad (1-1)$$

where the coefficient functions $\{\beta_j(t), j = 1, \dots, p\} \in (L^2[0, 1])^p$, and $\{(X_{jn}(t), \epsilon_n): j \geq 1\}$ are independent across n . More research works on functional linear models include, but are not limited to, Chiou et al. [4, 5, 6], Müller and Stadtmüller [28], Müller and Yao [29], Yao et al. [38], Ferraty et al. [12], Jiao and Ombao [19], Jiao et al. [16].

In gait analysis, coordination among different joints is pivotal for understanding human movement patterns and their underlying biomechanics. Existing research underscores the interdependence of angular kinematics, where the motion of one joint often influences or compensates for the movement of others to maintain balance, stability, and forward progression (see e.g., Ren et al. [33] and Dussault-Picard et al. [9]). Thus, an important task is to account for the interdependence among different covariates (i.e., the angular kinematics of various joints). Such interdependence often leads to covariates being associated with the response variable (e.g., chronological age) in a homogeneous manner. A reasonable strategy, therefore, is to group covariates based on the similarity of their effects on the response. Notable works in this area include Shen and Huang [35], Ke et al. [21], Ma and Huang [26], She et al. [34], and Jiao and Chan [17]. *However, ordinary grouping pursuit methods face a fundamental limitation: they rely on a uniform grouping structure.* For functional data, this restriction is inappropriate due to its infinite-dimensional nature. Specifically, different components of functional covariates may exhibit distinct grouping structures. Consequently, assuming a common structure can lead to model misspecification, reduced estimation efficiency, and hindered interpretability. Therefore, adopting flexible grouping strategies that accommodate variations in grouping structures across different dimensions is essential for accurate modeling and insightful interpretation.

1.3 Contributions and Novelties

The primary methodological contribution of this paper is the development of a filtration grouping algorithm for model (1-1), termed *filtrated grouping*, which allows for varying grouping structures across different dimensions. Here, we define “homogeneous components” as covariate components that share a common coefficient score in some dimension, reflecting their collective contribution to the response variable. The *key idea* is to iteratively filter out the homogeneous components of functional covariates that exhibit significant associations with the response variable, thereby constructing dimension-specific grouping structures. In the application, we employ the proposed methodology to examine the relationship between angular kinematics and chronological age for the healthy participants, with a particular focus on the coordination among different joints. The multi-resolutional coordination structure is discovered and highlights several important factors in the evaluation of effective age. The findings contribute to a deeper understanding of angular kinematics and offer a valuable tool for evaluating joint effective age, providing insights for enhancing age-related gait assessments and joint health evaluations.

This idea is inspired by filtration, a widely used technique in graph analysis and topological data analysis (see, e.g., Edelsbrunner et al. [10], Lee et al. [22], and Hofer et al. [15]), which iteratively constructs a sequence of nested structures and serves as a funda-

mental building block for multi-resolution analysis. However, it has been rarely applied in multivariate functional data analysis. To the best of our knowledge, the only related work is Jiao et al. [18], which employs filtration to construct a multi-resolution structure for partial common functional principal components (PCfPC), offering a more flexible and efficient representation of PCfPCs. This paper is the first work to develop filtration techniques for multiple functional regression.

The rest of the article is organized as follows. We present the filtrated grouping structure, and develop the model estimation procedure in Section 2. The identification of the filtrated grouping structure is discussed in Section 3. Simulation results are presented in Section 4. In Section 5, we apply our methods to analyze the association between chronological age and angular kinematics data. The paper is concluded in Section 6.

2 Filtrated multiple functional regression

2.1 Preliminaries

Notationally, let $X \in L_H^q = L_H^q(\Omega, \mathcal{A}, \mathcal{P})$ indicate that, for some $q > 0$, a H -valued function X satisfies $E\|X(t)\|^q < \infty$. In what follows, we assume that there are one scalar response y_n and p functional covariates $\{X_{jn}(t) \in L_H^2: j = 1, \dots, p\}$, where $H = L^2[0, 1]$ is equipped with the inner product $\langle x, y \rangle = \int_0^1 x(t)y(t)dt$ and the norm $\|x\|^2 = \int_0^1 x^2(t)dt$. It is assumed that $\{y_n, X_{jn}(t): j = 1, \dots, p\}$ are independent across $n = 1, \dots, N$. By Mercer's theorem, we have the following functional principal component decompositions $\mathcal{C}_j(\cdot) = \sum_{d \geq 1} \theta_{jd} \langle \nu_{jd}, \cdot \rangle \nu_{jd}(t)$, where $\mathcal{C}_j(x)(t) = \int \mathcal{C}_j(t, s)x(s)ds$ for $x \in L^2[0, 1]$, $\mu_j(t) = EX_{jn}(t)$, and $C_j(t, s) = E\{(X_{jn} - \mu_j)(t)(X_{jn} - \mu_j)(s)\}$. We assume that all the coefficient functions in (1-1) belong to the space spanned by $\{\nu_{jd}(t): d \geq 1, j \geq 1\}$.

Suppose that, for some sets of basis functions $\{\nu_{jd}(t) \in H: d \geq 1\}$ and $\{u_{jd}(t) \in H: d \geq 1\}$, the functional covariates and functional coefficients admit the following basis representation

$$X_{jn}(t) = \sum_{d \geq 1} \xi_{jn,d} \nu_{jd}(t), \quad \beta_j(t) = \sum_{d,d' \geq 1} b_{jd} M_{j,dd'} u_{jd'}(t),$$

in which the basis functions $\{\nu_{jd}(t): d \geq 1\}$ and $\{u_{jd}(t): d \geq 1\}$ can either be orthonormal or not. The term $M_j = \{M_{j,dd'}: d, d' \geq 1\}$ represents an infinite matrix satisfying the condition $\sum_{d' \geq 1} M_{j,d_1 d'} (\int \nu_{jd_2} u_{jd'}) = \mathbf{1}_{\{d_1=d_2\}}$. Then model (1-1) can be equivalently rewritten in the following form

$$y_n = \beta_0 + \sum_{d=1}^{\infty} \sum_{j=1}^p \xi_{jn,d} b_{jd} + \epsilon_n, \quad E\epsilon_n = 0, \quad \text{Var}(\epsilon_n) = \sigma^2. \quad (2-2)$$

For illustrating the filtrated grouping structure, we focus on the equivalent form (2-2), as the representation is dimension-specific (layer-specific), enabling a more precise characterization of grouping structures across different dimensions.

2.2 Filtrated Grouping Structure

Given a grouping structure $G = (\mathcal{K}_1, \dots, \mathcal{K}_m)$ satisfying $\mathcal{K}_i \cap \mathcal{K}_{i'} = \emptyset$ for $i \neq i'$ and $\cup_{i=1}^m \mathcal{K}_i = \{1, \dots, p\}$, the ordinary grouped model based on coefficient homogeneity is

$$y_n = \beta_0 + \sum_{i=1}^m \langle Z_{in}, \alpha_i \rangle + \epsilon_n, \quad \mathbb{E}\epsilon_n = 0, \quad \text{Var}(\epsilon_n) = \sigma^2, \quad (2-3)$$

where $Z_{in}(t) = \sum_{j \in \mathcal{K}_i} X_{jn}(t)$ and $\alpha_i(t)$ is the common coefficient function of group \mathcal{K}_i .

The ordinary model (1-1) cannot account for the homogeneity of functional coefficients and the estimation burden is high even for moderate p (see e.g., Jiao and Chan [17]). Although the grouped model (2-3) alleviates the estimation burden and improve model interpretability, it fails to capture variations in grouping structures across different dimensions. These limitations motivate the development of a more flexible modeling framework that can accommodate dimension-specific grouping variability.

Building upon the form (2-2), we develop the following filtrated grouping structure

$$y_n = \beta_0 + \sum_{d=1}^{\infty} \sum_{i=1}^{m_d} \left\{ \sum_{j \in \mathcal{K}_{d,i}} \xi_{jn,d} \right\} a_{d,i} + \epsilon_n, \quad \mathbb{E}\epsilon_n = 0, \quad \text{Var}(\epsilon_n) = \sigma^2, \quad (2-4)$$

where $\mathcal{K}_{d,i}$ denotes the i -th group in the d -th dimension/layer and m_d is the number of groups in the d -th dimension. We define the *homogeneous components* as follows

$$\zeta_{nd}^{(i)} \triangleq \sum_{j \in \mathcal{K}_{d,i}} \xi_{jn,d}, \quad i \geq 1, \quad d \geq 1,$$

and aim to estimate the associated coefficient scores $\{a_{d,i} : i \geq 1, d \geq 1\}$.

The coefficient homogeneity is captured in a multi-resolution manner, resulting in group indices $\{\mathcal{K}_{d,i} : i \geq 1, d \geq 1\}$ that follow a forest structure (see Figure 2). Compared to the ordinary grouped model (2-3), the filtrated grouped model (2-4) accommodates varying grouping structures across different dimensions. In the first layer, we identify the most homogeneous covariate components and group them accordingly to obtain $\{\zeta_{n1}^{(i)} : i \geq 1\}$ and estimate $\{a_{1,i} : i \geq 1\}$. After filtering out these homogeneous components from each covariate, we divide $\{\mathcal{K}_{1,i} : i \geq 1\}$ into $\{\mathcal{K}_{2,i} : i \geq 1\}$, which are either nested within or identical to the groups in the previous layer (i.e., for any $i \geq 1$, $\mathcal{K}_{2,i} \subseteq \mathcal{K}_{1,i'}$ for some $i' \geq 1$), and then obtain the homogeneous components in the new layer (i.e., $\{\zeta_{n2}^{(i)} : i \geq 1\}$) and estimate the associated coefficient scores (i.e., $\{a_{2,i} : i \geq 1\}$). The splitting procedure continues until a predefined stopping criterion is met. In the deeper layers of the filtration, higher-resolution homogeneous components, constructed from fewer covariates, are progressively extracted.

In the remainder of the article, we address the following problems: How to determine a reasonable forest structure for covariate grouping? Given the forest structure, how to identify homogeneous components and estimate coefficient scores? In Section 3, we

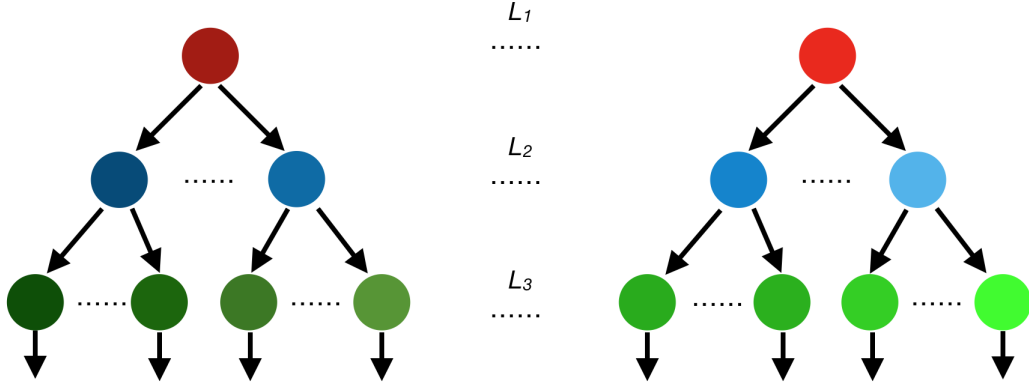


Figure 2: Hierarchical forest structure of coefficient homogeneity. Here, L_d signifies the d -th layer of filtration. Different groups are represented by different colored solid circles. Each group is either nested within or identical to its “parent” group in the previous layer, i.e., the group from which it originated through a split.

construct the forest structure based on the grouping path derived from the grouping pursuit problem, and in Section 2.3, we address the second problem by developing a filtrated functional partial least squares approach.

2.3 Filtrated Functional Partial Least Squares (filt-fPLS)

To identify the homogeneous components and estimate the coefficient scores, we developed a filtrated functional partial least squares method. To facilitate understanding of the proposed filt-fPLS algorithm, we begin with a simple illustrative case. In the ordinary grouped model (2-3), if $X_{1n}(t), \dots, X_{pn}(t) \in \mathcal{K}_1$ (i.e., all covariates belong to a single group \mathcal{K}_1), then we can estimate the model using the classical functional partial least squares approach (see Delaigle and Hall [8]), where $\sum_{j \in \mathcal{K}_1} X_{jn}(t)$ is treated as the covariate. The first step is to maximize $\text{cov}(y_n, \sum_{j \in \mathcal{K}_1} \langle X_{jn}, \psi \rangle)$ over $\psi(t)$, subject to the constraint $\|\psi\| = 1$. This is followed by a projection step, and the two steps are then repeated iteratively. In the filtrated grouped model (2-4), however, the grouping structure varies across dimensions. As a result, the maximization and projection steps are iteratively performed under different grouping configurations. The core principle of filt-fPLS is that the extracted homogeneous components should exhibit strong explanatory power for the response variable. We detail the algorithmic procedure below.

When $d = 1$, we first find the filt-fPLS basis for each group as follows,

$$\psi_{1,i}(t) \triangleq \arg \max_{\|\psi\|=1} \text{cov} \left\{ y_n, \left\langle \sum_{j \in \mathcal{K}_{1,i}} X_{jn}, \psi \right\rangle \right\} = \frac{\text{cov}\{y_n, \sum_{j \in \mathcal{K}_{1,i}} X_{jn}\}}{\|\text{cov}\{y_n, \sum_{j \in \mathcal{K}_{1,i}} X_{jn}\}\|}(t),$$

where $i = 1, \dots, m_1$. The m_1 first-layer homogeneous components are obtained as $\zeta_{n1}^{(i)} = \sum_{j \in \mathcal{K}_{1,i}} \int X_{jn} \psi_{1,i}$ for $i = 1, \dots, m_1$, and then estimate the associated coefficient scores:

$$\hat{a}_{1,i} = \arg \min_{\{a_{1,i} : i=1, \dots, m_1\}} \text{E} \left\{ y_n - \sum_{i=1}^{m_1} a_{1,i} \zeta_{n1}^{(i)} \right\}^2.$$

For $d \geq 2$, given $\{\psi_{d-1,i}(t) : i = 1, \dots, m_{d-1}\}$, the filt-fPLS basis for group $\mathcal{K}_{d,i}$ is

$$\psi_{d,i}(t) \triangleq \arg \max_{\|\psi\|=1} \text{cov} \left\{ y_n^{[d]}, \left\langle \sum_{j \in \mathcal{K}_{d,i}} X_{jn}^{[d]}, \psi \right\rangle \right\} = \frac{\text{cov}\{y_n^{[d]}, \sum_{j \in \mathcal{K}_{d,i}} X_{jn}^{[d]}\}}{\|\text{cov}\{y_n^{[d]}, \sum_{j \in \mathcal{K}_{d,i}} X_{jn}^{[d]}\}\|} (t).$$

Let $\zeta_{nd}^{(i)} = \sum_{j \in \mathcal{K}_{d,i}} \int X_{jn}^{[d]} \psi_{d,i}$, then obtain the associated coefficient scores as follows

$$\hat{a}_{d,i} = \arg \min_{\{a_{d,i} : i=1, \dots, m_d\}} \text{E} \left\{ y_n^{[d]} - \sum_{i=1}^{m_d} a_{d,i} \zeta_{nd}^{(i)} \right\}^2,$$

where

$$\begin{aligned} X_{jn}^{[d]}(t) &= X_{jn}^{[d-1]}(t) - \sum_{i=1}^{m_{d-1}} \zeta_{n,d-1}^{(i)} \phi_{d-1,i}(t), \\ \phi_{d,i}(t) &= \arg \min_{\{\delta_i(t) : i \geq 1\}} \text{E} \left\| X_{jn}^{[d]}(t) - \sum_{i=1}^{m_d} \zeta_{nd}^{(i)} \delta_i(t) \right\|^2, \\ y_n^{[d]} &= y_n^{[d-1]} - \sum_{i=1}^{m_{d-1}} \zeta_{n,d-1}^{(i)} \hat{a}_{d-1,i}, \end{aligned}$$

Particularly $X_{jn}^{[1]}(t) = X_{jn}(t)$, $y_n^{[1]} = y_n$.

It can be shown that under the forest structure, the homogeneous components across different layers are orthogonal (i.e., $\sum_{n \geq 1} \zeta_{nd}^{(i)} \zeta_{nd'}^{(i')} = 0$ for $d \neq d'$ and $i, i' \geq 1$). In practical applications, the unknown covariances and expectations are replaced by their empirical counterparts, as discussed in Algorithm 1.

3 Forest Structure Construction

The construction of the forest structure is based on the grouping path \mathcal{P} derived from the ordinary grouping pursuit problem. Specifically, this involves identifying $\mathcal{K}_1, \dots, \mathcal{K}_m$ in model (2-3) by solving a regularized optimization problem over a sequence of increasing penalty parameters (see e.g., Shen and Huang [35]), and \mathcal{P} encompasses all distinct grouping structures identified across different penalty parameters. Based on the grouping path, we first find a sequence of candidate grouping structures from which the forest structure is constructed. For the candidate grouping structures, it is required that the groups in each layer are nested within those of the preceding layer, as any non-nested grouping structures would complicate the construction of the forest structure. One challenge is that the grouping structures along the grouping path may not be nested as λ increases, due to the occurrence of group splitting. Thus, it is crucial to carefully select the candidate grouping structures from the grouping path.

In the following, we discuss the identification of grouping path in Section 3.1, the selection of candidate grouping structures in Section 3.2, and the construction of the forest structure in Section 3.3.

Algorithm 1 Filtrated functional partial least squares algorithm

- 1: Set $d = 1$, $X_{jn}^{[1]}(t) = X_{jn}(t)$, and $y_n^{[1]} = y_n$.
- 2: **while** the ending criterion (discussed in Section 3.3) is not met **do**
- 3: For $i = 1, \dots, m_d$, estimate $\psi_{d,i}(t)$ by

$$\hat{\psi}_{d,i}(t) = \sum_{n=1}^N \sum_{j \in \mathcal{K}_{d,i}} y_n^{[d]} X_{jn}^{[d]}(t) \bigg/ \left\| \sum_{n=1}^N \sum_{j \in \mathcal{K}_{d,i}} y_n^{[d]} X_{jn}^{[d]} \right\|.$$

- 4: Set $\zeta_{nd}^{(i)} = \sum_{j \in \mathcal{K}_{d,i}} \langle X_{jn}^{[d]}, \hat{\psi}_{d,i} \rangle$ and estimate the coefficient scores by least squares

$$\hat{a}_{d,i} = \arg \min_{\{a_{d,i}: i=1, \dots, m_d\}} \sum_{n=1}^N \left\{ y_n^{[d]} - \sum_{i=1}^{m_d} a_{d,i} \zeta_{nd}^{(i)} \right\}^2.$$

- 5: Obtain the residuals

$$\begin{aligned} X_{jn}^{[d+1]}(t) &= X_{jn}^{[d]}(t) - \sum_{i=1}^{m_d} \zeta_{nd}^{(i)} \hat{\phi}_{d,i}(t), \\ \hat{\phi}_{d,i}(t) &= \arg \min_{\{\delta(t): i \geq 1\}} \sum_{n=1}^N \left\| X_{jn}^{[d]}(t) - \sum_{i=1}^{m_d} \zeta_{nd}^{(i)} \delta_i(t) \right\|^2, \\ y_n^{[d+1]} &= y_n^{[d]} - \sum_{i=1}^{m_d} \hat{a}_{d,i} \zeta_{nd}^{(i)}. \end{aligned}$$

- 6: $d = d + 1$
 - 7: **end while**
-

3.1 Grouping Path

The grouping pursuit problem is formulated by optimizing the objective function:

$$S(\boldsymbol{\beta}(t), \lambda) = \frac{1}{2} \sum_{n=1}^N \left(y_n - \sum_{j=1}^p \langle X_{jn}, \beta_j \rangle \right)^2 + \sum_{i < j} J_\lambda(\|\beta_i - \beta_j\|),$$

where $\boldsymbol{\beta}(t) = \{\beta_j(t): 1 \leq j \leq p\}$, and $J_\lambda(\cdot)$ is some concave penalty, such as the SCAD penalty (see Fan and Li [11]) and the MCP (see Zhang [39]). As λ increases, covariates tend to be clustered into fewer groups, although sometimes grouping splitting may occur. The sequence of grouping structures that emerge as the regularization parameter λ increases defines the *grouping path* \mathcal{P} .

Suppose that for some orthonormal basis functions $\{\nu_d(t): d \geq 1\}$, the following basis representations hold: $X_{jn}(t) = \sum_{d \geq 1} \xi_{jn,d} \nu_d(t)$ and $\beta_j(t) = \sum_{d \geq 1} b_{jd} \nu_d(t)$. Since $S(\boldsymbol{\beta}(t), \lambda)$ involves elements of infinite dimensions, we minimize the following truncated

version over $\{b_{jd}: d = 1, \dots, D, j \geq 1\}$ with some sufficiently large $D \geq 1$,

$$S_D(\boldsymbol{\beta}(t), \lambda) = \frac{1}{2} \sum_{n=1}^N \left(y_n - \sum_{j=1}^p \boldsymbol{\xi}_{jn}^\top \mathbf{B}_j \right)^2 + \sum_{i < j} J_\lambda(\|\mathbf{M}_{ij}\|), \quad (3-5)$$

where $\boldsymbol{\xi}_{jn} = (\xi_{jn,1}, \dots, \xi_{jn,D})^\top$, $\mathbf{B}_j = (b_{j1}, \dots, b_{jD})^\top$ and $\mathbf{M}_{ij} = \mathbf{B}_i - \mathbf{B}_j$. We use the ADMM algorithm to solve (3-5). Let $\mathbf{B} = \{\mathbf{B}_j: j = 1, \dots, p\}$, $\mathbf{M} = \{\mathbf{M}_{ij}: i < j\}$, and

$$H_1(\mathbf{B}) = \frac{1}{2} \sum_{n=1}^N \left(y_n - \sum_{j=1}^p \boldsymbol{\xi}_{jn}^\top \mathbf{B}_j \right)^2, \quad H_2(\mathbf{M}) = \sum_{i < j} J_\lambda(\|\mathbf{M}_{ij}\|),$$

then the unconstrained optimization problem is equivalent to the following constrained optimization problem

$$H(\mathbf{B}, \mathbf{M}) = H_1(\mathbf{B}) + H_2(\mathbf{M}), \text{ subject to } \mathbf{M}_{ij} = \mathbf{B}_i - \mathbf{B}_j, \ 1 \leq i < j \leq p. \quad (3-6)$$

By the ADMM algorithm, the regularized estimates of \mathbf{B}, \mathbf{M} can be obtained by minimizing the augmented Lagrangian function

$$L_\theta(\mathbf{B}, \mathbf{M}, \mathbf{u}) = H(\mathbf{B}, \mathbf{M}) + \sum_{i < j} \mathbf{u}_{ij}^\top (\mathbf{B}_i - \mathbf{B}_j - \mathbf{M}_{ij}) + \frac{\theta}{2} \sum_{i < j} \|\mathbf{B}_i - \mathbf{B}_j - \mathbf{M}_{ij}\|^2$$

over \mathbf{B} and \mathbf{M} . Given \mathbf{B} and multipliers $\mathbf{u} = \{u_{ij,dd'}, i < j, d < d'\}$, we update \mathbf{M} by minimizing $L_\theta(\mathbf{B}, \mathbf{M}, \mathbf{u})$ over \mathbf{M} , and the optimization problem is equivalent to minimizing the following function over \mathbf{M} ,

$$\frac{\theta}{2} \sum_{i < j} \|\mathbf{M}_{ij} - (\mathbf{B}_i - \mathbf{B}_j) - \theta^{-1} \mathbf{u}_{ij}\|^2 + \sum_{i < j} J_\lambda(\|\mathbf{M}_{ij}\|). \quad (3-7)$$

For $j = 1, \dots, p$, define $\boldsymbol{\Xi}_j = (\boldsymbol{\xi}_{1j}, \dots, \boldsymbol{\xi}_{Nj})^\top$, $\boldsymbol{\Xi} = (\boldsymbol{\Xi}_1 | \dots | \boldsymbol{\Xi}_p)$. The minimizer of \mathbf{B} given \mathbf{M} and \mathbf{u} of the augmented Lagrangian function is

$$\mathbf{B} = (\boldsymbol{\Xi}^\top \boldsymbol{\Xi} + \theta \boldsymbol{\Delta}^\top \boldsymbol{\Delta})^{-1} (\boldsymbol{\Xi}^\top \mathbf{y} + \theta \boldsymbol{\Delta}^\top (\mathbf{M} - \theta^{-1} \mathbf{u})). \quad (3-8)$$

Here, $\boldsymbol{\Delta} = (\boldsymbol{\Delta}_{ij}, i < j)$ represents the matrix formed by concatenating the row blocks $\boldsymbol{\Delta}_{ij}$, and $\boldsymbol{\Delta}_{ij} = (\dots, \mathbf{0}, \mathbf{I}, \mathbf{0}, \dots, \mathbf{0}, -\mathbf{I}, \mathbf{0}, \dots)$ is a $d \times pd$ matrix where \mathbf{I} is the $d \times d$ identity matrix. We summarize the above discussion in Algorithm 2.

3.2 Candidate Grouping Structures

After obtaining the grouping path \mathcal{P} , we first construct candidate sets of grouping structures from the path, from which the forest structure is constructed. Notationally, for two grouping structures G, G' , $G \subseteq G'$ means that every group in G is nested in some group in G' . Denote a candidate set by $\mathcal{G} = \{G_1, \dots, G_\ell\}$, where ℓ is the number of grouping structures in \mathcal{G} , and $G_i \in \mathcal{P}$ denotes the i -th layer's grouping structure of the candidate set \mathcal{G} satisfying $G_\ell \subseteq G_{\ell-1} \subseteq \dots \subseteq G_1$.

Algorithm 2 The ADMM algorithm for grouping pursuit

- 1: Initialize estimates $\mathbf{B}^{(0)}$ (e.g., ordinary least squares estimate of \mathbf{B}) and set $\mathbf{u}^{(0)} = \mathbf{0}$.
 - 2: **while** convergence criterion is not met **do**
 - 3: Given $\mathbf{B}^{(m)}$ and $\mathbf{u}^{(m)}$, calculate $\mathbf{M}^{(m+1)}$ by minimizing (3-7) over \mathbf{M} .
 - 4: Given $\mathbf{M}^{(m+1)}$ and $\mathbf{u}^{(m)}$, calculate $\mathbf{B}^{(m+1)}$ using (3-8).
 - 5: Update the multipliers $u_{ij,dd'}^{(m+1)} = u_{ij,dd'}^{(m)} + \theta \{b_{id}^{(m+1)} - b_{jd}^{(m+1)} - M_{ij,d}^{(m+1)}\}$.
 - 6: **end while**
 - 7: **return** $\mathbf{B}^{(m+1)}$.
-

Multiple candidate sets can be constructed from the grouping path, and only one of them is used for constructing the forest structure of model (2-4). The relationship $\mathcal{G} \subseteq \mathcal{G}'$ means that every grouping structure in \mathcal{G} is also included in \mathcal{G}' . To make the candidate set as inclusive as possible, we require that any two different candidate sets $\mathcal{G} = \{G_1, \dots, G_\ell\}$ and $\mathcal{G}' = \{G'_1, \dots, G'_{\ell'}\}$ satisfy that a) $\mathcal{G} \not\subseteq \mathcal{G}'$ and $\mathcal{G}' \not\subseteq \mathcal{G}$, b) $G_1 = G'_1 = \{1, 2, \dots, p\}$, and $G_\ell = G'_{\ell'} = \{\{1\}, \{2\}, \dots, \{p\}\}$. The selected candidate set should ensure sufficient diversity in grouping structures to support forest construction and achieve strong predictive performance in the resulting model. We now present the procedure for selecting the candidate set.

1. **Initial Construction:** Construct all candidate sets that satisfy conditions (a) and (b) from the grouping path \mathcal{P} .
2. **Set Evaluation:** For each candidate set, we construct the grouped model (2-3) based on all grouping structures in the set and estimate the prediction error using a resampling-based method (e.g., cross-validation, bootstrap).
3. **Final Selection:** Compute the average prediction error of the models built across all grouping structures within each candidate set and select the one that yields the lowest average prediction error.

This selection procedure ensures that the chosen candidate set represents a comprehensive forest hierarchy, capturing the finest level of details available in the grouping process. Meanwhile, the grouping structures in the selected candidate set retain strong explanatory power, thereby aligning with the covariance maximization principle central to filt-fPLS.

3.3 Iterative Selection of Grouping Structures

The forest structure is constructed from the selected candidate set $\tilde{\mathcal{G}} = \{\tilde{G}_1, \dots, \tilde{G}_\ell\}$ through an iterative process. Specifically, starting from the first layer, we sequentially examine all the grouping structure in the selected candidate set $\tilde{G}_1, \dots, \tilde{G}_\ell$. If, based on a predefined criterion, the grouping structure selected for the current layer is \tilde{G}_i , the process continues to the next layer by sequentially testing $\tilde{G}_i, \dots, \tilde{G}_\ell$.

We develop a generalized information criterion (GIC, see e.g., Nishii [30] and Zhang et al. [40]) to select the grouping structures across different layers. The format of GIC criterion is: $\text{GIC} = \text{measure of model fit} + \text{tuning parameter} \times \text{measure of model com-}$

plexity. In principle, if the covariates are separated into too many groups, the resulting grouping structure would fail to explain the covariate interdependence. Therefore, we penalize complex grouping structure. Notationally, denote a forest structure by \mathcal{F} , and $F_d \in \tilde{\mathcal{G}}$ as the d -th layer's grouping structure in \mathcal{F} . We develop an iterative GIC criterion, with the layer-wise GIC value defined as

$$\text{GIC}(F_d) = N^{-1} \sum_{n=1}^N (y_n^{[d+1]})^2 + \tau_d |F_d|,$$

where $|F_d|$ denotes the number of groups in F_d , and $y_n^{[d+1]}$'s are the $(d+1)$ -th layer's response residuals in the filt-fPLS procedure based on the grouping structure F_d . We select F_d to minimize $\text{GIC}(F_d)$. Here, $\{\tau_d: d \geq 1\}$ is a non-increasing sequence with respect to d , thus the number of groups tends to increase as d increases. Clearly, denote $\tilde{\mathcal{F}}$ as the identified forest structure, we have the relationship $\tilde{\mathcal{F}} \subseteq \tilde{\mathcal{G}} \subseteq \mathcal{P}$.

The number of tuning parameters $\{\tau_d: d \geq 1\}$ increases with d , making tuning parameter selection increasingly complicated when the total number of layers is large. To achieve efficient tuning parameter adaptation, we propose adopting a parametric form for τ_d , for example, $\tau_\theta(d) = \rho\gamma^{-d+1}$, where $\theta = (\rho, \gamma)$. Using a parametric form significantly reduces the computational burden, as it requires selecting only θ rather than individually determining each τ_d .

Ending criterion. Now we discuss how to fix the maximal layer of the forest structure. In principle, the filtration should continue until the extracted homogeneous components no longer significantly improve the response's fitting error. Thus, we propose the following ending criterion: we stop filtration at the d -th layer if $\sum_n \{(y_n^{[d]})^2 - (y_n^{[d+1]})^2\} / \sum_n (y_n^{[d]})^2 < e$, where $e > 0$ is a small value. If $\sum_n \|X_{jn}^{[d+1]}\|^2$ becomes sufficiently small, we remove the j -th covariate from further filtration.

4 Simulation

4.1 General Setting

In this section, we investigate the finite-sample performance of filtrated grouping. It is important to emphasize that, although our simulation is based on a pre-specified forest structure, the objective is *not* to exactly recover the structure. Rather, the goal is to identify a suitable structure that highlights the numerical advantages of the filtrated grouping framework. The oracle structure is never known in practice, and the forest-structured groups are difficult to fully recover. Nevertheless, our simulation results demonstrate that even when the oracle structure is not fully recovered, the selected forest structure still effectively (even superiorly) captures the underlying homogeneity.

We simulate N samples for the following multiple functional regression model with 10 covariates $\{X_{jn}(t): j = 1, \dots, 10\}$, $y_n = \sum_{j=1}^{10} \langle X_{jn}, \beta_j \rangle + \epsilon_n$, where $\epsilon_n \stackrel{i.i.d.}{\sim} \mathcal{N}(0, \sigma^2)$ and $\sigma = 0.3, 0.5, 0.7, 1.0$. The covariate and coefficient functions are simulated by the

following basis expansion,

$$X_{jn}(t) = \sum_{d=1}^D \xi_{jn,d} B_d(t), \quad \beta_j(t) = \sum_{d=1}^D b_{jd} B_d(t),$$

where $\{B_d(t): d \geq 1\}$ are the Fourier basis functions. The scores $\xi_{jn,d}$ follow the standard normal distribution and are independent across n , j and d . To facilitate the detection of coefficient homogeneity among the tail scores, we do not impose any decay on the covariate score variance. Here we set $D = 9$, and the coefficient scores $\{b_{jd}: j = 1, \dots, 10, d = 1, \dots, D\}$ are displayed in Figure 3.

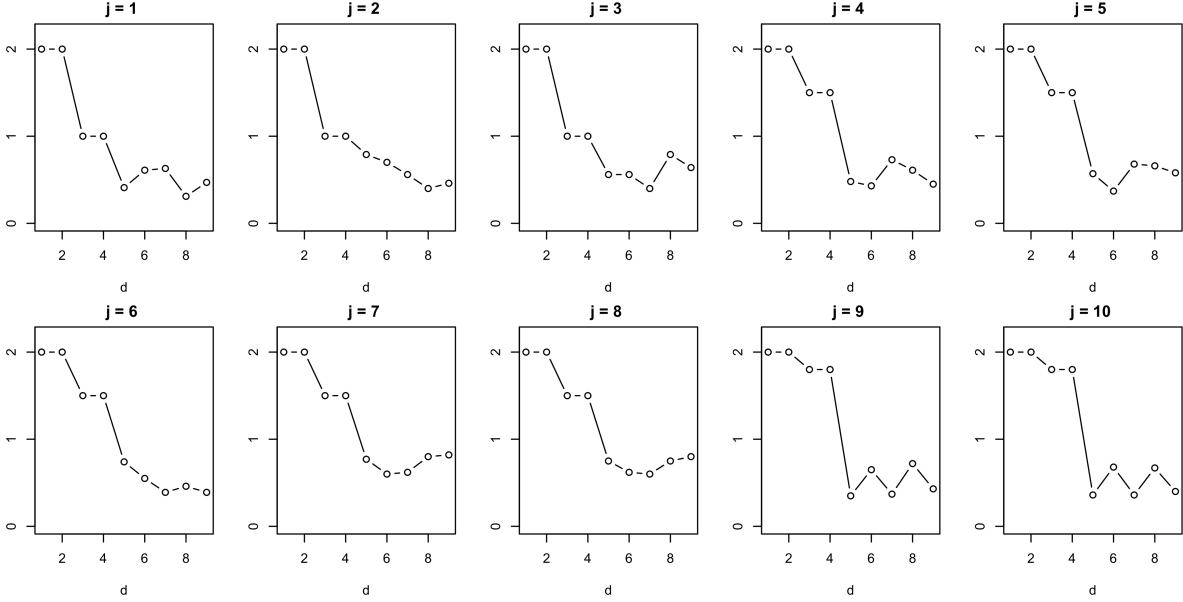


Figure 3: Coefficient scores $\{b_{jd}: d = 1, \dots, D\}$ of the 10 coefficients.

Note that the coefficient scores exhibit partial homogeneity. Specifically, the first two scores are set to 2 for all $j = 1, \dots, p$, reflecting the global homogeneity shared by all covariates. The third and fourth scores are identical within certain subsets of covariates: they are the same for covariates 1 – 3, covariates 4 – 8, and covariates 9 – 10. The last five scores are all different across j , reflecting the idiosyncratic effects of different covariates. The ℓ^2 -distance between different pairs of coefficient score vectors are displayed in Table 1.

In this setting, the homogeneity among the 10 coefficient functions cannot be captured by a fixed grouping structure, as the homogeneity across different dimensions is characterized by varying grouping structures. The homogeneity is represented by the forest structure shown in Figure 4. However, this structure may not be optimal. Small differences between $\beta_4(t)$ and $\beta_5(t)$, $\beta_7(t)$ and $\beta_8(t)$, as well as $\beta_9(t)$ and $\beta_{10}(t)$, could cause these pairs to be merged across more layers in the identified forest structure.

$i \backslash j$	2	3	4	5	6	7	8	9	10
1	0.166	0.337	0.638	0.720	0.699	0.993	0.919	1.523	1.495
2	*	0.283	0.742	0.754	0.562	0.804	0.748	1.616	1.582
3	*	*	0.701	0.635	0.704	0.627	0.607	1.382	1.408
4	*	*	*	0.034	0.224	0.298	0.260	0.387	0.400
5	*	*	*	*	0.222	0.174	0.158	0.429	0.455
6	*	*	*	*	*	0.357	0.301	0.412	0.386
7	*	*	*	*	*	*	0.004	0.580	0.615
8	*	*	*	*	*	*	*	0.532	0.560
9	*	*	*	*	*	*	*	*	0.005

Table 1: $\sum_{d \geq 1} (b_{id} - b_{jd})^2$ for $1 \leq i < j \leq 10$.

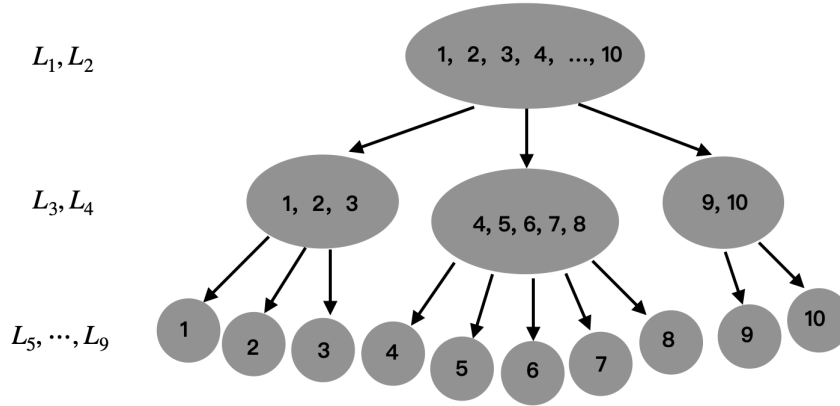


Figure 4: The oracle forest structure underlying coefficient homogeneity.

4.2 Forest Structure Identification

We set $N = 400$ and $\sigma = 0.5$. The identified forest structure is given in Table 2. The associated filt-fPLS basis functions are displayed in Figure 5. The filt-fPLS basis functions reveal the common kinematics patterns shared by joints in the same group. For instance, global homogeneity is positively driven by the collective influence of covariates during the intervals 0–0.4 and 0.95–1 of the domain. It is noted that only in the first layer all covariates are clustered into the same group. This global homogeneous component is driven by the first two layers of the oracle structure. In the second layer, the 4th to 10th covariates are clustered together due to their closer values of b_{jd} . Specifically, as $d = 3, 4$, $b_{jd} = 1.5$ for $j = 4, \dots, 8$ and $b_{jd} = 1.8$ for $j = 9, 10$, and these values are relatively closer to each other compared to $b_{jd} = 1$ for $j = 1, 2, 3$. In the 3rd and 4th layers, the closeness between $\beta_4(t)$ and $\beta_5(t)$, $\beta_7(t)$ and $\beta_8(t)$, as well as $\beta_9(t)$ and $\beta_{10}(t)$, leads to these pairs of covariates being clustered in the same group. In the final layer, the structure captures the individual contributions of each covariate. Overall, the identified forest structure closely aligns with the oracle forest structure and captures the underlying homogeneity more efficiently, as it comprises only six layers and delivers substantially better predictive performance (see Section 4.3).

$d \backslash j$	1	2	3	4	5	6	7	8	9	10
1	1	1	1	1	1	1	1	1	1	1
2	1	1	1	2	2	2	2	2	2	2
3	1	2	3	4	4	5	6	6	7	7
4	1	2	3	4	4	5	6	6	7	7
5	1	2	3	4	5	6	7	7	8	8
6	1	2	3	4	5	6	7	8	9	10

Table 2: The identified group indices $c_{j,d}$ of different covariates.

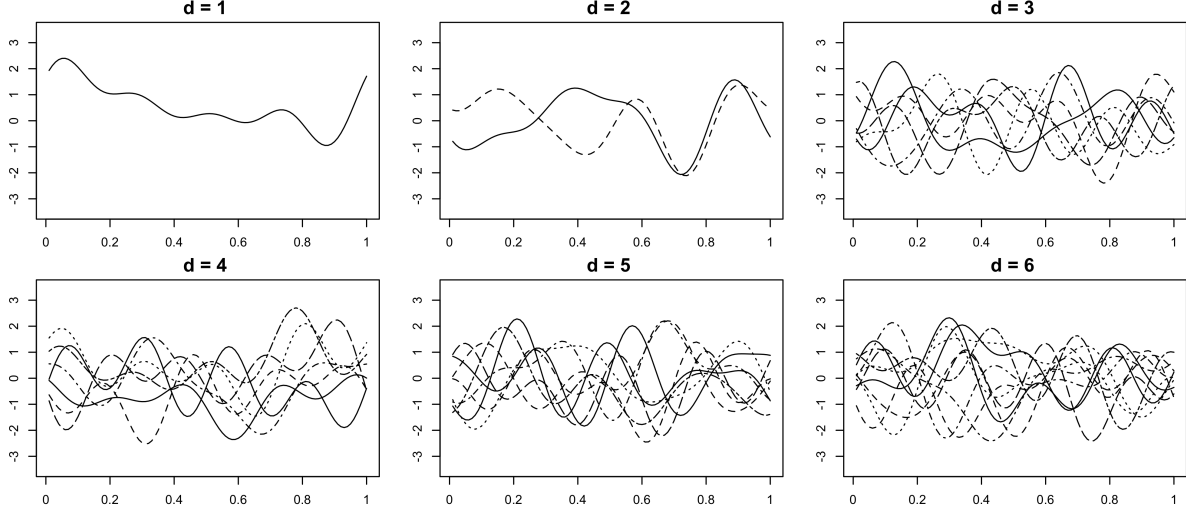


Figure 5: The estimated fPLS basis functions for all the 6 layers.

4.3 Model Performance and Comparison

To illustrate the superiority of the new filtrated modeling procedure, we compare the prediction performance of the following methods: 1). MFR based on the identified forest structure (Identified); 2). MFR based on the oracle forest structure (Oracle); 3). Grouped multiple function regression (Grouped, see 2-3); 4). MFR based on the naive grouping structure (NPLS), where no covariates are clustered together in all layers. We test this naive structure to show the necessity of grouping; 5). Ordinary multiple functional linear regression (MFLR).

We repeat 300 simulation runs for each simulation setup. In each run, we generate either 100 or 300 samples for the training set to train the model, and 200 additional samples in the test set used for prediction. The prediction mean squared error (MSE), calculated as $MSE = \sum_{n=1}^{200} (\hat{y}_n - y_n)^2 / 200$, is computed for each simulation run. As a result, a total of 300 prediction MSE values are obtained.

The box plots of prediction MSEs are presented in Figure 6. They clearly demonstrate that the identified grouping structure outperforms the oracle structure in capturing the relationship between covariates and the response. Its substantial superior-

ity over the naive structure underscores the importance of grouping. As a baseline, the ordinary multiple functional regression model performs the worst. Although the grouped model performs reasonably well, it still falls short compared to the filtrated grouped model. This is because the homogeneity among functional covariates is multi-resolutional, making a fixed grouping structure across different layers inappropriate. Interestingly, although the data are generated based on the oracle structure, the identified forest structure yields significantly better performance. This improvement arises because the data-driven structure more effectively captures the underlying mechanisms of the data. In particular, covariates exhibiting subtle nuances may be better modeled within the same group, thereby rendering the oracle structure suboptimal.

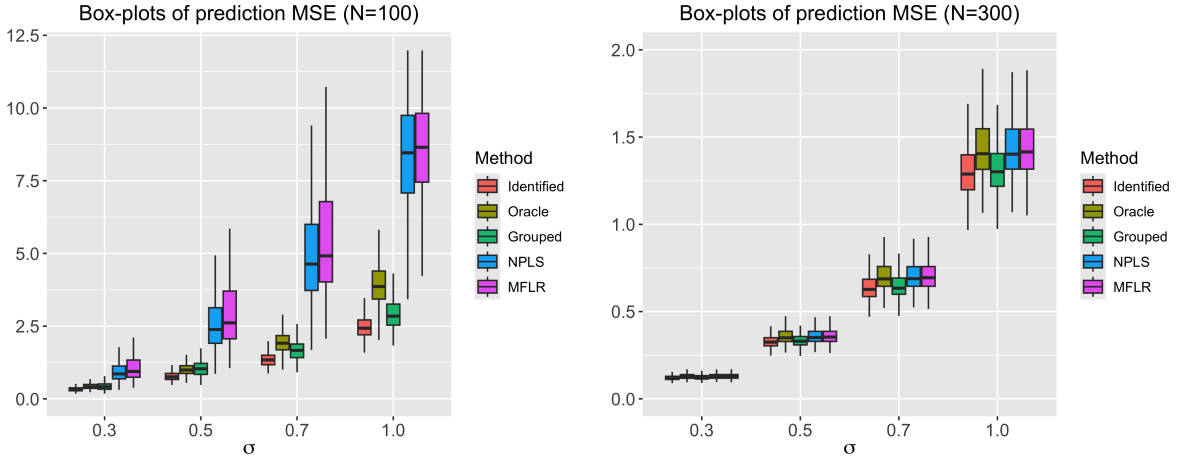


Figure 6: Prediction MSEs of different methods.

5 Effective Age and Angular Kinematics

In this study, we explore the relationship between the chronological age and the angular kinematics for the healthy participants in the experiment (see Fukuchi et al. [14]), driven by its relevance to communicating chronic risk analysis. The aim of this study is to develop a model-based system for evaluating the “effective age” of joints, which reflects joint functional health and aging.

5.1 Data Summary, Pre-processing, and Modeling Setup

We average the angular kinematic functions collected from the left and right sides to reduce model complexity. Consequently there are 15 functional covariates, including pelvic obliquity, pelvic rotation, pelvic tilt, hip add/abduction, hip int/external rotation, hip flexion/extension, knee add/abduction, knee int/external rotation, knee flx/extension, ankle inv/eversion, ankle add/abduction, ankle dorsi/plantarflexion, foot inv/eversion, foot int/external rotation and foot DF/plantarflexion angles (see Figure 7). To facilitate the forest structure identification and improve model interpretability, we centralize the log-transformed age and use it as the response, and we scale the

covariates (angular kinematics curves) as follows,

$$\tilde{X}_{jn}(t) = \frac{X_{jn}(t) - \bar{X}_j(t)}{\sqrt{N^{-1} \sum_{n=1}^N \|X_{jn}(t) - \bar{X}_j(t)\|^2}},$$

where $\bar{X}_j(t) = N^{-1} \sum_{n=1}^N X_{jn}(t)$. The participants were required to walk on treadmill under different gait speeds, which are categorized into four groups: 40–55% (S1), 70–85% (S2), 100–115% (S3), and 130–145% (S4) of the normal walking speed. Then we establish models under different gait speeds. Due to page limitations, the results, except those in Section 5.4, focus on the 100–115% normal walking speed range.

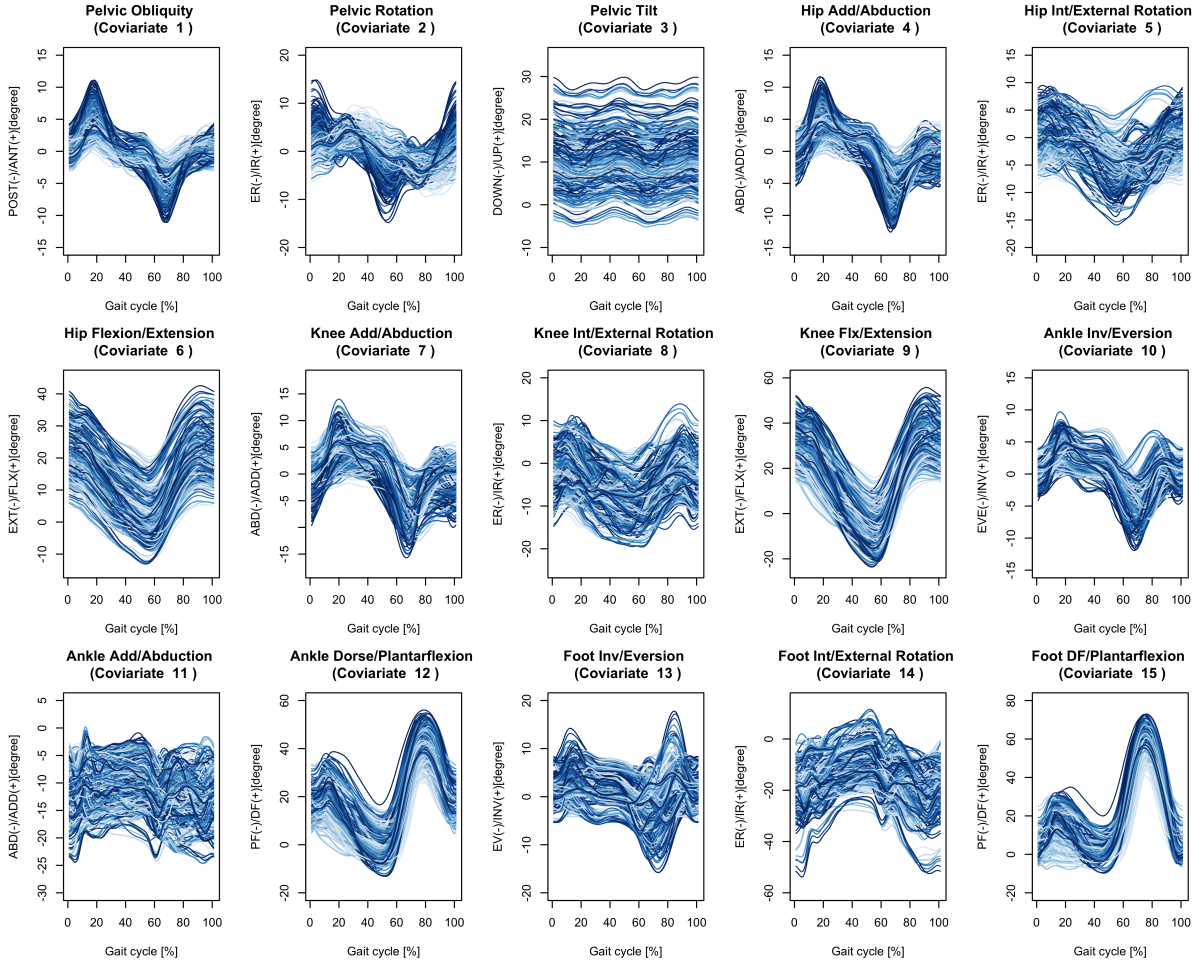


Figure 7: Joint angular kinematics functions averaged across the left and right sides, with curve colors indicating walking speed as shown in Figure 1.

5.2 Forest Structure Identification

We employ a Monte Carlo cross-validation approach to select the tuning parameters in the GIC criterion. Specifically, the data is randomly split into a training set (80%)

and a test set (20%). The model trained on the training set is used to predict the responses in the test set. We repeat this procedure 1000 times to obtain the average prediction MSE. The tuning parameters θ associated with the minimal prediction MSE is then used for forest structure identification, resulting in the forest structure displayed in Figure 8. The group indices are displayed as follows:

- $\tilde{\mathcal{F}}_1$. $\mathcal{K}_{1,1}$: covariate 1, 4; $\mathcal{K}_{1,2}$: covariate 2, 3, 5, \dots , 15;
- $\tilde{\mathcal{F}}_2$. $\mathcal{K}_{2,1}$: covariate 1; $\mathcal{K}_{2,2}$: covariate 2, 3, 5, 6, 8, \dots , 15; $\mathcal{K}_{2,3}$: covariate 4; $\mathcal{K}_{2,4}$: covariate 7;
- $\tilde{\mathcal{F}}_3$. $\mathcal{K}_{3,i}$: covariate i , for $i = 1, \dots, p$;
- $\tilde{\mathcal{F}}_4$. $\mathcal{K}_{4,1}$: covariate 2; $\mathcal{K}_{4,2}$: covariate 5; $\mathcal{K}_{4,3}$: covariate 10; $\mathcal{K}_{4,4}$: covariate 11; $\mathcal{K}_{4,5}$: covariate 13; $\mathcal{K}_{4,6}$: covariate 14; $\mathcal{K}_{4,7}$: covariate 15;
- $\tilde{\mathcal{F}}_5$. $\mathcal{K}_{5,1}$: covariate 11.

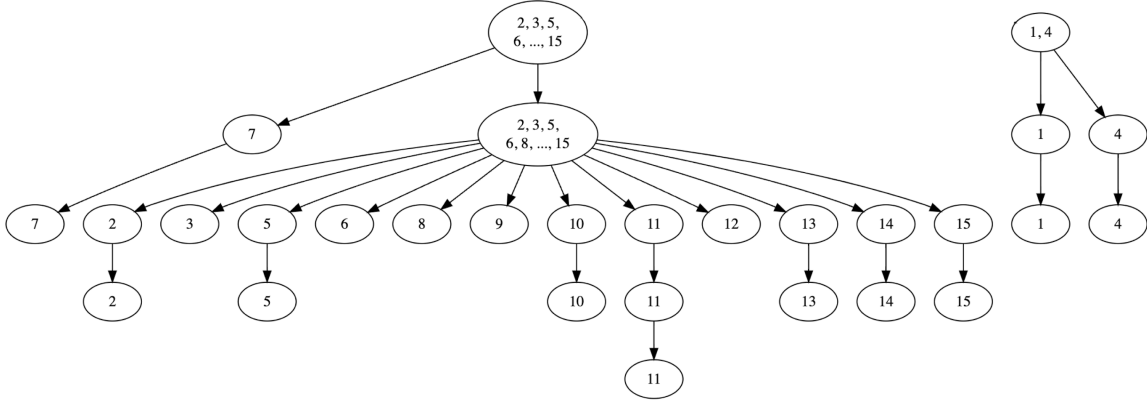


Figure 8: The identified forest structure under 100–115% normal walking speed (the numbers in the circles represent the covariate indices). There are five layers in total. Most covariates are removed from Layers 4 and 5, as the extracted homogeneous components already account for a substantial proportion of their variation.

The forest structure reveals that the associations of pelvis obliquity and hip adduction/abduction with age differ substantially from those of other joints, as they are separated at the first layer. This separation reflects their unique adaptations to age-related changes in gait and balance control. In addition, knee add/abduction also demonstrates significant distinctiveness, leading to its separation in the second layer. In contrast, the kinematics of most other joints exhibit a high degree of interdependence, suggesting more uniform adaptations to preserve forward propulsion and overall gait efficiency.

5.3 Homogeneous Components

The filt-fPLS basis functions $\psi_{d,i}(t)$ reveal how the homogeneous components are associated with age. Figure 9 presents the filt-fPLS basis functions in the first two layers. These basis functions reflect how the homogeneous components are affected by the relevant angular kinematics. For instance, in the first layer, the homogeneous component of group 1 is positively determined by the related angular kinematics (pelvis

obliquity and hip adduction/abduction) during 40–70% of the gait cycle and negatively affected during the remainder of the gait cycle. The homogeneous components of group 2 (driven by all other joints) is uniformly positively determined by the related angular kinematics.

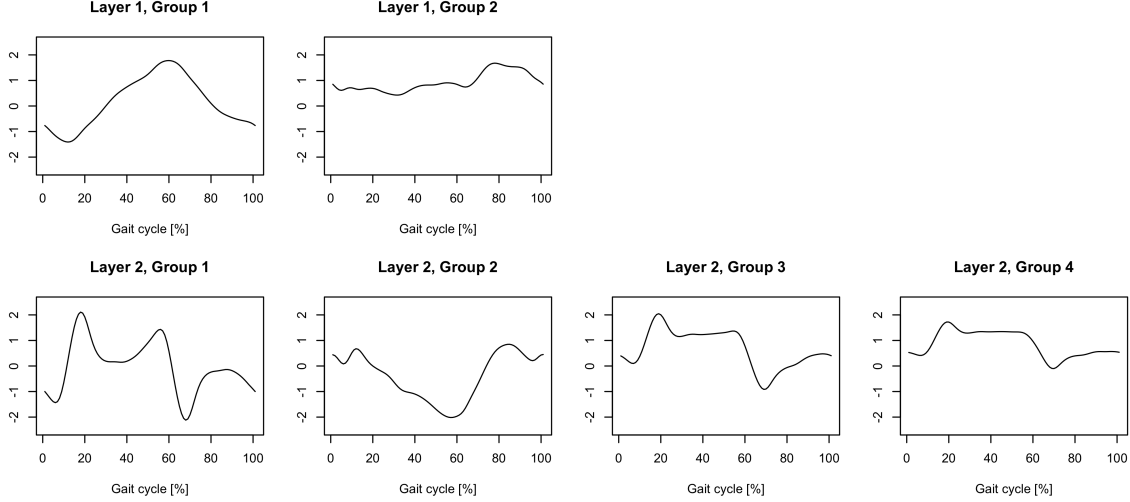


Figure 9: The partial least square basis functions in the first two layers $\{\psi_{d,i}(t) : d = 1, 2, i \geq 1\}$.

Define the model component of the i -th group in the d -th layer as $a_{d,i}\zeta_{nd}^{(i)}$. We display the 95% confidence interval of the coefficient scores $\{a_{d,i} : i, d \geq 1\}$ and the standard deviation of the associated model components in Figure 10. The upper panel, which shows the confidence interval of the coefficient scores, highlights how different homogeneous components are associated with the response. The homogeneous components in the first layer, corresponding to the two sets of joints, both exhibit positive associations with the response, and in the second layer, all homogeneous components except for the one related to hip add/abduction are also positively associated with the response.

Interestingly, the results reveal a prominent spike in variation for hip flexion/extension. This suggests that the idiosyncratic gait patterns of hip flexion/extension plays a crucial role in reflecting the effective age. As people grow older, there’s a well-documented distal-to-proximal shift in gait: propulsion and control move away from ankle and knee toward hip. This shift makes hip movement a central driver of gait, so its variability becomes especially telling (see e.g., Franz and Kram [13]). Certain homogeneous components are found to be non-significant in the model. Specifically, the idiosyncratic components in the third layer associated with pelvic obliquity, pelvic rotation, knee adduction/abduction, knee internal/external rotation, knee flexion/extension, and ankle dorsiflexion/plantarflexion show negligible associations with age.

5.4 Predictive Power

In this section, we evaluate the predictive performance of the filtrated model, developed under various gait speed levels categorized in Section 5.1, in predicting the chronological

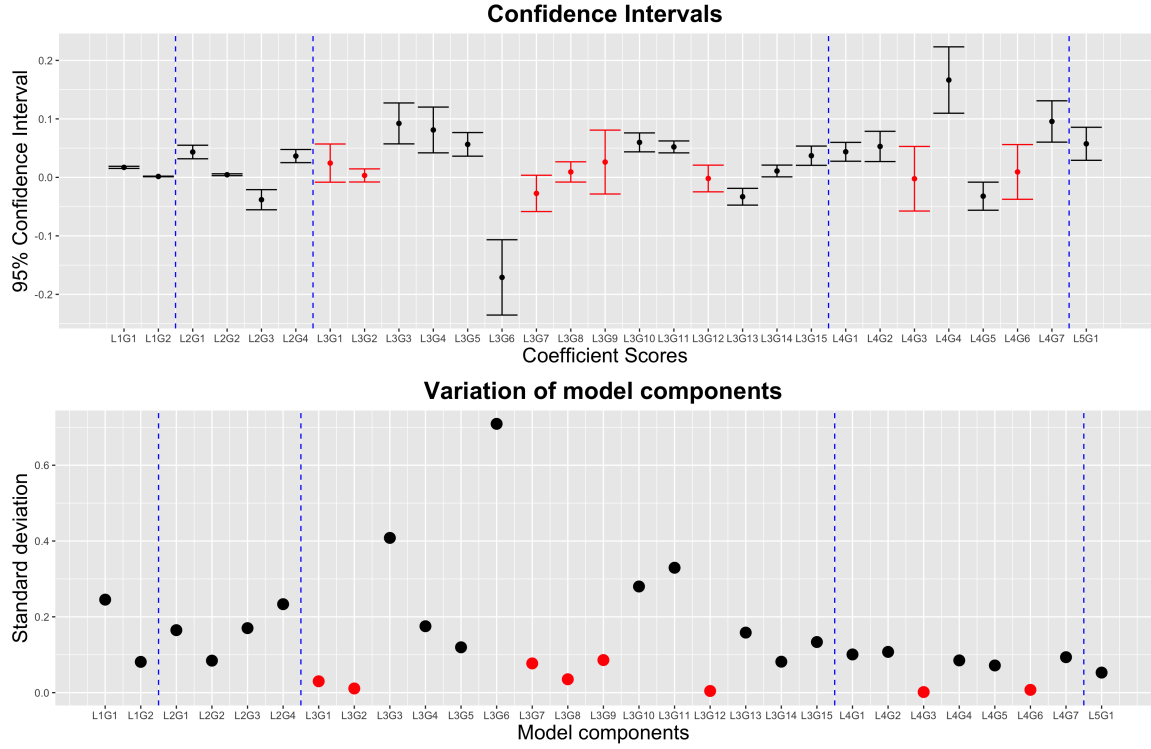


Figure 10: The confidence intervals for coefficient scores and the standard deviation of model components. Different layers are separated by blue dashed lines. $LiGj$ represents the j -th group in the i -th layer. The insignificant homogeneous components are marked in red.

age. We compare the proposed method with two competing approaches: the grouped functional regression model (2-3) and the ordinary functional regression model (1-1). We use the same Monte Carlo cross-validation approach to evaluate predictive performance, and the prediction MSEs are shown in Figure 11. The results indicate that the filtrated model achieves the best performance at 70–80% of normal walking speed, suggesting that participants should be encouraged to walk at a slightly slower pace than their natural, comfortable speed when assessing their joint effective age.

The filtrated model consistently provides the most accurate and robust predictions. In contrast, the ordinary model underperforms due to its high complexity, which leads to substantial estimation errors and diminished predictive power. While the grouped model demonstrates improved performance over the ordinary model, it remains suboptimal compared to the filtrated model. This discrepancy arises because the idiosyncratic components across different covariates exhibit significant variation. Treating these heterogeneous components collectively, as in the grouped model, fails to capture their distinct contributions, thereby limiting predictive accuracy.

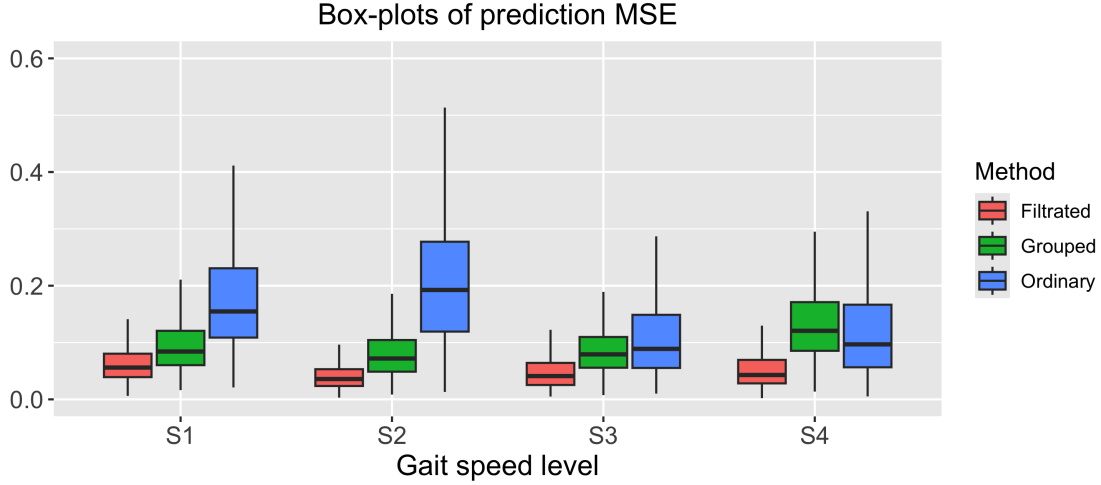


Figure 11: Box-plots of MSEs of different methods. The variance of the response variable under the four gait speed levels is 0.19, 0.19, 0.19, and 0.17, respectively.

6 Conclusion

We propose a novel filtrated grouping procedure for multiple functional regression models with a scalar response and multiple functional covariates, addressing the challenges posed by the joint coordination and joint effective age evaluation. By introducing a forest-structured grouped model and a data-driven filtrated partial least squares estimation procedure, our approach effectively captures both homogeneous and idiosyncratic effects of covariates from a multi-resolution perspective. Our results demonstrate the potential of this framework to uncover biomechanical adaptations and mechanisms associated with joint aging. By hierarchically grouping covariates, the method has the ability to identify both homogeneous and idiosyncratic features across different joints provides a comprehensive understanding of the interdependence in gait dynamics, supporting the evaluation of effective age and facilitating informed decision-making in clinical and research settings. The proposed approach surpasses existing methods in both interpretability and predictive accuracy, and provides a comprehensive modeling framework for complex covariate relationships.

This study marks the first effort to integrate filtration techniques into multiple functional regression, and our results underscore the substantial potential and impact of this approach. The framework is inherently generalizable and can be extended to other applications involving multiple functional covariates. Future work will broaden the filtration paradigm to other functional methodologies—such as functional factor models and classification frameworks.

References

- [1] Anderson, A. S. and Loeser, R. F. [2010], ‘Why is osteoarthritis an age-related disease?’, *Best practice & research Clinical rheumatology* **24**(1), 15–26.

- [2] Cao, C., Cao, J., Wang, H., Tsui, K.-L. and Li, X. [2013], ‘Functional adaptive double-sparsity estimator for functional linear regression model with multiple functional covariates’, *Statistica Sinica* **36**(2), 04.2026.
- [3] Cheng, Y., Shi, J. Q. and Eyre, J. [2020], ‘Nonlinear mixed-effects scalar-on-function models and variable selection’, *Statistics and Computing* **30**(1), 129–140.
- [4] Chiou, J.-M., Müller, H.-G. and Wang, J.-L. [2003], ‘Functional quasi-likelihood regression models with smooth random effects’, *Journal of the Royal Statistical Society Series B: Statistical Methodology* **65**(2), 405–423.
- [5] Chiou, J.-M., Müller, H.-G. and Wang, J.-L. [2004], ‘Functional response models’, *Statistica Sinica* pp. 675–693.
- [6] Chiou, J.-M., Yang, Y.-F. and Chen, Y.-T. [2016], ‘Multivariate functional linear regression and prediction’, *Journal of Multivariate Analysis* **146**, 301–312.
- [7] Dannenmaier, J., Kaltenbach, C., Kölle, T. and Krischak, G. [2020], ‘Application of functional data analysis to explore movements: walking, running and jumping-a systematic review’, *Gait & Posture* **77**, 182–189.
- [8] Delaigle, A. and Hall, P. [2012], ‘Methodology and theory for partial least squares applied to functional data’, **40**(1), 322–352.
- [9] Dussault-Picard, C., Cherni, Y., Ferron, A., Robert, M. and Dixon, P. [2023], ‘The effect of uneven surfaces on inter-joint coordination during walking in children with cerebral palsy’, *Scientific Reports* **13**(1), 21779.
- [10] Edelsbrunner, H., Harer, J. et al. [2008], ‘Persistent homology-a survey’, *Contemporary mathematics* **453**(26), 257–282.
- [11] Fan, J. and Li, R. [2001], ‘Variable selection via nonconcave penalized likelihood and its oracle properties’, *Journal of the American statistical Association* **96**(456), 1348–1360.
- [12] Ferraty, F., Van Keilegom, I. and Vieu, P. [2012], ‘Regression when both response and predictor are functions’, *Journal of Multivariate Analysis* **109**, 10–28.
- [13] Franz, J. R. and Kram, R. [2013], ‘Advanced age affects the individual leg mechanics of level, uphill, and downhill walking’, *Journal of biomechanics* **46**(3), 535–540.
- [14] Fukuchi, C. A., Fukuchi, R. K. and Duarte, M. [2018], ‘A public dataset of over-ground and treadmill walking kinematics and kinetics in healthy individuals’, *PeerJ* **6**, e4640.
- [15] Hofer, C., Graf, F., Rieck, B., Niethammer, M. and Kwitt, R. [2020], Graph filtration learning, in ‘International Conference on Machine Learning’, PMLR, pp. 4314–4323.
- [16] Jiao, S., Aue, A. and Ombao, H. [2023], ‘Functional time series prediction under partial observation of the future curve’, *Journal of the American Statistical Association* **118**(541), 315–326.

- [17] Jiao, S. and Chan, N.-H. [2024], ‘Coefficient shape alignment in multiple functional regression’, *Journal of the American Statistical Association* (just-accepted), 1–21.
- [18] Jiao, S., Frostig, R. and Ombao, H. [2024], ‘Filtrated common functional principal component analysis of multigroup functional data’, *The Annals of Applied Statistics* **18**(2), 1160–1177.
- [19] Jiao, S. and Ombao, H. [2021], ‘Shape-preserving prediction for stationary functional time series’, *Electronic Journal of Statistics* **15**(2), 3996–4026.
- [20] Kay, R. M., Dennis, S., Rethlefsen, S., Skaggs, D. L. and Tolo, V. T. [2000], ‘Impact of postoperative gait analysis on orthopaedic care’, *Clinical Orthopaedics and Related Research*® **374**, 259–264.
- [21] Ke, Z. T., Fan, J. and Wu, Y. [2015], ‘Homogeneity pursuit’, *Journal of the American Statistical Association* **110**(509), 175–194.
- [22] Lee, H., Chung, M. K., Kang, H., Kim, B.-N. and Lee, D. S. [2011], Computing the shape of brain networks using graph filtration and gromov-hausdorff metric, in ‘Medical Image Computing and Computer-Assisted Intervention–MICCAI 2011: 14th International Conference, Toronto, Canada, September 18–22, 2011, Proceedings, Part II 14’, Springer, pp. 302–309.
- [23] Li, Y., Wei, X., Zhou, J. and Wei, L. [2013], ‘The age-related changes in cartilage and osteoarthritis’, *BioMed research international* **2013**(1), 916530.
- [24] Loeser, R. F. [2010], ‘Age-related changes in the musculoskeletal system and the development of osteoarthritis’, *Clinics in geriatric medicine* **26**(3), 371.
- [25] Loftørød, B., Terjesen, T., Skaaret, I., Huse, A.-B. and Jahnsen, R. [2007], ‘Pre-operative gait analysis has a substantial effect on orthopedic decision making in children with cerebral palsy: comparison between clinical evaluation and gait analysis in 60 patients’, *Acta orthopaedica* **78**(1), 74–80.
- [26] Ma, S. and Huang, J. [2017], ‘A concave pairwise fusion approach to subgroup analysis’, *Journal of the American Statistical Association* **112**(517), 410–423.
- [27] Morris, J. S. [2015], ‘Functional regression’, *Annual Review of Statistics and Its Application* **2**, 321–359.
- [28] Müller, H.-G. and Stadtmüller, U. [2005], ‘Generalized functional linear models’, *The Annals of Statistics* **33**(2), 774–805.
- [29] Müller, H.-G. and Yao, F. [2008], ‘Functional additive models’, *Journal of the American Statistical Association* **103**(484), 1534–1544.
- [30] Nishii, R. [1984], ‘Asymptotic properties of criteria for selection of variables in multiple regression’, *The Annals of Statistics* pp. 758–765.
- [31] Ramsay, J. O. and Silverman, B. W. [2004], ‘Functional data analysis’, *Encyclopedia of Statistical Sciences* **4**.

- [32] Rao, A. K., Muratori, L., Louis, E. D., Moskowitz, C. B. and Marder, K. S. [2008], ‘Spectrum of gait impairments in presymptomatic and symptomatic huntington’s disease’, *Movement disorders: official journal of the Movement Disorder Society* **23**(8), 1100–1107.
- [33] Ren, X., Lutter, C., Keibach, M., Bruhn, S., Bader, R. and Tischer, T. [2022], ‘Lower extremity joint compensatory effects during the first recovery step following slipping and stumbling perturbations in young and older subjects’, *BMC geriatrics* **22**(1), 656.
- [34] She, Y., Shen, J. and Zhang, C. [2022], ‘Supervised multivariate learning with simultaneous feature auto-grouping and dimension reduction’, *Journal of the Royal Statistical Society Series B: Statistical Methodology* **84**(3), 912–932.
- [35] Shen, X. and Huang, H.-C. [2010], ‘Grouping pursuit through a regularization solution surface’, *Journal of the American Statistical Association* **105**(490), 727–739.
- [36] Spiegelhalter, D. [2016], ‘How old are you, really? communicating chronic risk through ‘effective age’ of your body and organs’, *BMC medical informatics and decision making* **16**, 1–6.
- [37] Wang, B., Luo, X., Zhao, Y. and Caffo, B. [2019], ‘Semiparametric partial common principal component analysis for covariance matrices’, *Biometrics* pp. 1175–1186.
- [38] Yao, F., Müller, H.-G. and Wang, J.-L. [2005], ‘Functional data analysis for sparse longitudinal data’, *Journal of the American Statistical Association* **100**(470), 577–590.
- [39] Zhang, C.-H. [2010], ‘Nearly unbiased variable selection under minimax concave penalty’, *The Annals of Statistics* **38**(2), 894–942.
- [40] Zhang, Y., Li, R. and Tsai, C.-L. [2010], ‘Regularization parameter selections via generalized information criterion’, *Journal of the American Statistical Association* **105**(489), 312–323.
- [41] Zhou, J., Wang, N.-Y. and Wang, N. [2013], ‘Functional linear model with zero-value coefficient function at sub-regions’, *Statistica Sinica* **23**(1), 25–50.